frontiers in Materials

ORIGINAL RESEARCH
published: 04 December 2020
doi: 10.3389/fmats.2020.549002

Preparation and Ultrasonic Imaging Investigation of Perfluoropentane-Filled Polylactic Acid Nanobubbles As a Novel Targeted Ultrasound Contrast Agent

Ruolei Xiao[1†], Zhiwei Zhao[2†], Jiajuan Chen[3†], Liu He[1], Huili Wang[1], Lingping Huang[4] and Binhua Luo[1*]*

[1]School of Pharmacy, Hubei University of Science and Technology, Xianning, China, [2]Department of Radiology, Xianning Central Hospital, The First Affiliated Hospital of Hubei University of Science and Technology, Xianning, China, [3]Department of Cardiology, Taihe Hospital, Hubei University of Medicine, Shiyan, China, [4]Department of Medical Ultrasound, Xianning Central Hospital, The First Affiliated Hospital of Hubei University of Science and Technology, Xianning, China

OPEN ACCESS

Edited by:
Kai-Xue Wang,
Shanghai Jiao Tong University, China

Reviewed by:
M. Gabriella Santonicola,
Sapienza University of Rome, Italy
Jie-Sheng Chen,
Shanghai Jiao Tong University, China

***Correspondence:**
Binhua Luo
lbh9811015@163.com
Lingping Huang
xnhlp2012@163.com

[†]These authors have contributed equally to this work

Specialty section:
This article was submitted to Colloidal Materials and Interfaces, a section of the journal Frontiers in Materials

Received: 21 April 2020
Accepted: 02 November 2020
Published: 04 December 2020

Citation:
Xiao R, Zhao Z, Chen J, He L, Wang H, Huang L and Luo B (2020) Preparation and Ultrasonic Imaging Investigation of Perfluoropentane-Filled Polylactic Acid Nanobubbles As a Novel Targeted Ultrasound Contrast Agent. Front. Mater. 7:549002. doi: 10.3389/fmats.2020.549002

In the study reported here, polylactic acid (PLLA) polymer was synthesized using stannous octoate ($Sn(Oct)_2$) and N-(t-butoxycarbonyl) ethanolamine (EABoc) as the catalyst and the initiator, respectively. The selected PLLA polymer with proper molecular weight was used to prepare nanobubbles encapsulating with liquid perfluoropentane. Then, lactoferrin (Lf), which has a good affinity with tumor cells, was conjugated to PLLA nanobubbles. The resulting Lf–PLLA nanobubbles were examined from the perspective of appearance, size, zeta potential, and stability *in vitro*. The average hydrodynamic diameter of the Lf–PLLA nanobubbles was 315.3 ± 4.2 nm, the polydispersity index (PDI) was 0.153 ± 0.020, and the zeta potential was around −11.3 ± 0.2 mV. Under the transmission electron microscope (TEM), Lf–PLLA nanobubbles were highly dispersed and had a spherical shape with a distinct capsule structure. The Lf–PLLA nanobubbles also showed little cytotoxicity and low hemolysis rate and exhibited good stability *in vitro*. The enhanced ultrasound imaging ability of Lf–PLLA nanobubbles was detected by an ultrasound imaging system. The results of ultrasound studies *in vitro* showed that the liquid perfluoropentane underwent phase transition under ultrasonic treatment, which proved the Lf–PLLA nanobubbles could enhance the ability of ultrasonic imaging. The studies of ultrasonic imaging in nude mice bearing subcutaneous tumors showed that the ability of enhanced ultrasonic images was apparent after injection of Lf–PLLA nanobubbles. Acoustic behavior *in vitro* and *in vivo* showed that the Lf–PLLA nanobubbles were characterized by strong, stabilized, and the ability of tumor-enhanced ultrasound imaging. Thus, the Lf–PLLA nanobubbles are an effective ultrasound contrast agent for contrast-enhanced imaging.

Keywords: polylactic acid, nanobubbles, contrast agent, *in vivo* ultrasound imaging, *in vitro* acoustic behavior

INTRODUCTION

Noninvasive ultrasound imaging technology has been widely used in clinics, which can be performed with real-time imaging (Xie et al., 2016b). Ultrasound (US) imaging is based on the reflection of US waves at the interfaces between materials and/or tissues (Guvener et al., 2017). With the development of sensor technology and the application of novel ultrasound pulse sequences, especially when the image postprocessing strategies are improved, the sensitivity of US has been dramatically raised. However, for areas with slow blood vessels, or the early stage of illness, contrast-enhanced ultrasonic imaging is required to enhance the visibility of US imaging. Ultrasound contrast agents are needed tools for clinical contrast-enhanced ultrasound imaging. As commercial contrast agents, microsized bubble of around 1–8 μm have been typically employed in contrast-enhanced US imaging. The increase in the US signal is due to the acoustic impedance between blood or surrounding tissue and the gas of microbubbles. Besides, under certain mechanical index of ultrasonic irradiation, microbubbles undergo cavitation or produce volumetric oscillations and are destroyed, which will transiently increase cellular membrane permeability and can create pores in the target region (Perera et al., 2013; Zhu et al., 2017). Therefore, gas-filled microbubbles are considered as a promising vehicle for drug/gene delivery, which can facilitate extravascular delivery and drug release in addition to the diagnostic application (Zhao and Lu, 2007; Wang et al., 2009; Zhang et al., 2011; Tranquart et al., 2014; Wu et al., 2018). However, for their large size, microbubbles can only be served as blood pool contrast agents and pose a serious limitation in ultrasonic imaging of extravascular tissues (Guvener et al., 2017; Li et al., 2017a).

In recent years, nanobubbles (NBs) with lipids or polymers as the carrier material have attracted researchers to explore extravascular US imaging and exhibited good contrast enhancement (Ji et al., 2014; Cai et al., 2015; Yang et al., 2015a; Zhu et al., 2018). The vascular endothelial cells in normal tissues have a closer endothelial junction. However, tumor tissues usually form a defective vascular system with large gaps. In fact, for a variety of tumors, the characteristic pore cutoff size ranges from 360 to 780 nm. Therefore, NBs have enhanced permeability and retention, which can effectively accumulate in the interstitium of a tumor and naturally become a promising ultrasound contrast agent for tumor imaging and treatment (Meng et al., 2016; Nishimura et al., 2017; Song et al., 2017; Zhou et al., 2018).

Recently, nanobubbles (NBs) with a variety of shells consisting albumin, lipids, nonionic surfactants, and polymers have been applied in extravascular ultrasonic imaging (Yao et al., 2016; Duan et al., 2017; Gao et al., 2017; Du et al., 2018). Due to their surface characteristics, small size, and novel physical properties, nanobubbles composed of the polymer can gain access to the extravascular space, which provides special advantages for US imaging of targeted tissues; furthermore, the hard shell of polymers makes nanobubbles more stable and thus have longer circulation life (Zhang et al., 2014; Li et al., 2017b). However, the mechanical strength and degradation time are related to the molecular weight of the polymer. The higher the polymer molecular weight is, the stronger the mechanical strength appears, the more difficult it will be to destroy nanobubbles, so their properties make it difficult to satisfy the needs of a new drug/gene carrier. In addition, there are no active sites on these polymers, adding difficulty in conjugating the targeting groups.

Biodegradable polymers are widely used in drug carriers and biological tissue engineering materials, which are decomposed into nontoxic metabolites *in vivo*. Aliphatic polymers, such as polylactic acid and polyglycolic acid, are most extensively studied and widely used (Wu et al., 2017; Dinh Nguyen et al., 2018; Cai et al., 2019). In recent years, polylactic acid has attracted much attention because of its wide application in the biomedical field. Furthermore, the degraded monomers are easily metabolized by normal metabolic pathways and are excreted from the body without harming humans, which makes it a successful candidate material for drug delivery and which has been approved by the FDA as an excipient for drugs (Yang et al., 2015b; He et al., 2019; Tonietto et al., 2019). The conventional synthetic method that uses polylactide is the ring-opening polymerization (ROP) of lactide catalyzed by stannous octoate, which results in well-controlled molecular weight and low polydispersity. In the study reported here, poly(lactic acid) with controllable molecular weight was polymerized by ring-opening polymerization (ROP) of L-lactide. The obtained poly(lactic acid) was used as the carrier material to prepare NBs encapsulating liquid perfluoropentane (PFP) with double-emulsion solvent evaporation method. Lactoferrin (Lf), which has a good affinity with glioma cells, was used as a tumor-targeted group to conjugate nanobubbles. The physiochemical characteristics of resulting Lf–PLLA nanobubbles, such as appearance, hydrodynamic size, zeta potential, and stability *in vitro*, were investigated. The biocompatibility of Lf–PLLA nanobubbles was evaluated by the hemolysis test and cytotoxicity assay. The phase change behavior was triggered by ultrasound and acoustic waves *in vivo* and *in vitro* of the Lf–PLLA nanobubbles, which was performed with clinical ultrasound imaging equipment.

MATERIALS AND METHODS

L-lactide was obtained from Daigang Biomaterial Co, Ltd (Jinan, China). Poly(vinyl alcohol) (PVA-217) was purchased from Kuraray Co, Ltd (Tokyo, Japan). Perfluoropentane was purchased from JenKem Technology Co, Ltd (Beijing, China); di-tert-butyl dicarbonate, ethanolamine, and stannous octoate were obtained from Aladdin Chemistry (Shanghai, China); lactoferrin (Lf) from bovine colostrum was purchased from Sigma Chemical Co (St Louis, MO, USA).

Synthesis of N-(T-Butoxycarbonyl) Ethanolamine

N-(t-butoxycarbonyl) ethanolamine (EABoc) was synthesized using the method as described previously (Luo et al., 2015).

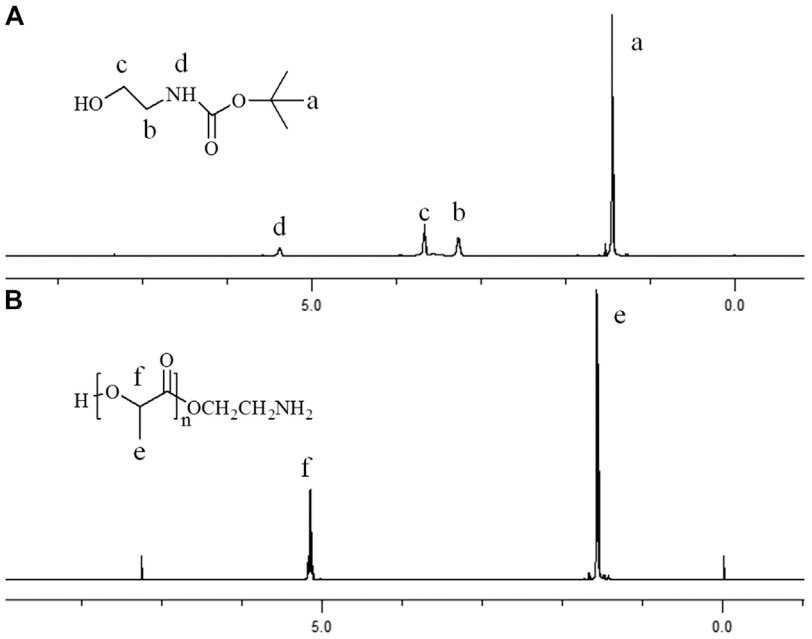

Figure 1 | Proton nuclear magnetic resonance spectra (in CDC_{13}, ppm) of **(A)** EABoc, **(B)** poly(L-lactide).

Briefly, 0.01 mol of sodium bicarbonate in 10 ml water was mixed with 0.01 mol of ethanolamine in tetrahydrofuran (10 ml) at 0°C. Then, 0.01 mol of di-tert-butyl dicarbonate was dripped over a period of 30 min with electromagnetic stirring. The mixture was stirred for another 8 h at 25°C and extracted with diethyl ether. Afterward, the organic solvents were collected and dried with enough anhydrous sodium sulfate. N-(t-butoxycarbonyl) ethanolamine (EABoc) was obtained by rotary decompression evaporation. **Figure 1A** shows the ^1H NMR spectra of EABoc.

Synthesis of Amine-Terminated Polylactic Acid

PLLA was synthesized using $Sn(Oct)_2$ and EABoc as the catalyst and the initiator, respectively. A certain proportion of L-lactide (recrystallized with dry ethyl acetate three times), EABoc, and $Sn(Oct)_2$ was added to a high-purity nitrogen-purged three-necked round-bottomed flask. At 120°C, the mixture was kept to react for 3 h. After the reaction, 5 ml chloroform was added and the product was dissolved. Afterward, the resulting product precipitated into cold methanol solution; precipitates were collected and washed with methanol twice. Finally, the precipitates were dried overnight under vacuum at 40°C. The molecular weight of PLLA was measured by gel permeation chromatography.

Formation and Targeting Modification of PLLA NBs

Traditional double-emulsion solvent evaporation method was used to prepare PLLA nanobubbles. PLLA (0.05 g) was added to 1 ml of chloroform, which was used as an O_2 phase. At low temperature, PFP (0.5 ml) was added to the O_2 phase, and the solution was stirred at 10,000 rpm for 3 min to form a primary emulsion ($O_1/O_{2)}$. Then, the resulting emulsion was poured into 0.5% PVA solution (10 ml) to obtain the coarse double emulsion under stirring condition , followed by sonication for 5 min with a probe-type sonicator at 100 W in an ice bath. Chloroform was evaporated by gentle stirring for 8 h at room temperature; therefore, nanobubbles were obtained. The PLLA NBs were centrifuged and dispersed in normal saline solution. Lf that exhibited a good affinity with glioma cells was conjugated to PLLA NBs according to our previous works (Luo et al., 2015), and then, the preparation of targeted modified nanobubbles (Lf–PLLA NBs) was complete.

Measurement of Lf–PLLA Nanobubbles Characteristics

The average hydrodynamic size and zeta potential of the Lf–PLLA nanobubbles were determined by dynamic light scattering (Malvern, UK) with a laser wavelength of 633 nm at 25°C, with the angle of 90°. The morphological visualization of the Lf–PLLA nanobubbles was characterized by TEM (Tokyo, Japan) with an acceleration voltage of 100 kV.

Cell Culture

The human normal liver cell line (HL-7702) and rat C6 glioma (C6) cell line were obtained from the Shanghai Institute of Life Science Cell Resource Center (Shanghai, China). Cells were cultured in DMEM containing 10% FBS in a humidified atmosphere of 5% CO_2 at 37°C.

Cytotoxicity Assay *In Vitro*

The cytotoxicity of Lf–PLLA nanobubbles on HL-7702 cells was determined by the MTT assay. Cells were seeded at a density of 5,000 cells per well in 96-well plates containing DMEM medium. After overnight incubation, the cells were continuously incubated with fresh medium containing different concentrations of nanobubbles (0.0%, 0.5%, 1.0%, 2.5%, 5.0%, 7.5%, 10.0%, 12.5%, 15.0%, and 20.0%, v/v) for another 24 h. PBS was used as the control group. The absorbance of each well was recorded at 492 nm on a multimode plate reader (Beyotime Biotechnology, Nantong, China).

Hemolysis *In Vitro*

Arterial blood was collected from male SD rats. The blood samples were centrifuged (2000 rpm, 10 min) to remove fibrinogen and washed with PBS until the supernatant was clear. Erythrocyte suspension (2%, v/v) was obtained by dilution with normal saline. Lf–PLLA NBs were added to erythrocyte suspension and produced mixture at various concentrations (0.5%, 1.0%, 2.5%, 5.0%, 7.5%, 10.0%, 12.5%, 15.0%, 20.0%, v/v). Furthermore, a mixture of erythrocyte suspension (150 μl) and normal saline (150 μl) was used as the negative control group, and a mixture of erythrocyte suspension (150 μl) and double-distilled water (150 μl) was used as the positive control group. After being incubated at 37°C in a water bath for 1 h, the samples were centrifuged at 4°C. The resulting supernatant was measured at 540 nm with a spectrophotometer. The ratio of hemolysis was calculated by using the following equation:

$$\text{Hemolysis ratio} = \frac{A_{sample} - A_{negative}}{A_{positive} - A_{negative}} \times 100\%$$

Ultrasound Imaging *In Vitro*

To evaluate the acoustic behavior of the Lf–PLLA nanobubbles, ultrasonic imaging experiments *in vitro* were performed with clinical ultrasound imaging equipment (Philips IU22, Amsterdam, Netherlands). Lf–PLLA NB solution was added to the latex gloves, which were immersed in a thermostatic water bath. Subsequently, the 10 MHz probe touched gloves to collect ultrasonic images. Image postprocessing analysis was performed with Photoshop software. The contrast strength of the nanobubbles was compared with that of the normal saline and ultrasonic medicinal coupling gel.

Ultrasound-Enhanced Tumor Imaging With Lf-PLLA NBs *In Vivo*

All animal use and relevant experimental procedures abided by the Guidelines of Animal Experimentation of Hubei University of Science and Technology. Male BALB/c nude mice weighing 18–20 g at 4 weeks of age were purchased from the Animal Center at Tongji Medical College. C6 cells (3×10^6) were suspended in phosphate buffer (100 μl) and inoculated subcutaneously into nude mice to establish animal models.

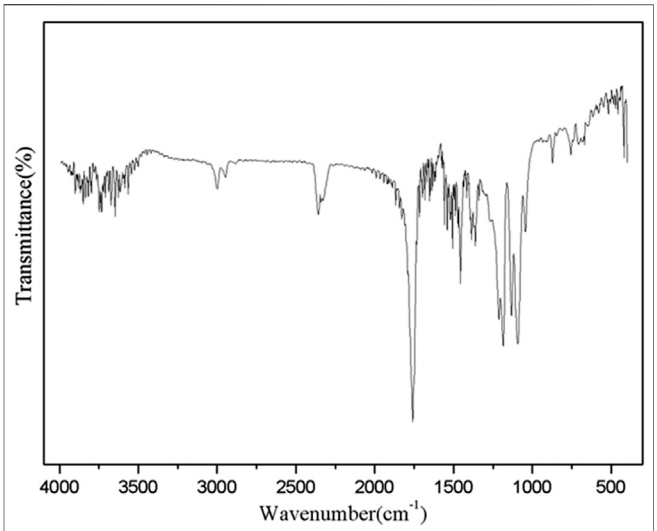

Figure 2 | FTIR spectra of polylactic acid polymer.

When the tumor diameter reached about 0.8 cm, the experiments *in vivo* were performed.

Tumor-bearing nude mice (n = 6) were anesthetized intraperitoneally with chloral hydrate and fixed on a heated plate to maintain their body temperature. Ultrasonic medicinal coupling gel was used to connect the tumor tissue with the probe to avoid the existence of air between them. First, the probe was placed on the region of the tumor of nude mice and detected the tumors with a fixed mechanical index (MI) value (0.08). The obtained images were used as control. Then, 100 μl of Lf–PLLA NBs were injected into each tumor-bearing nude mice, respectively. The instrument parameters remained unchanged during the experiment, and all images were saved for offline inspection.

Statistical Method

Statistical analysis was performed using unpaired Student's *t*-test. All data were expressed as mean ± SD.

RESULTS AND DISCUSSION

In this work, $Sn(Oct)_2$ was used as the catalyst for cyclic ester polymerization of L-lactide with EABoc as initiator, and amine-terminated polylactic acid (Mn = 12,000) was obtained. The products were characterized by ^1H NMR spectroscopy and the FTIR spectra. The peak at 1.53 ppm corresponds to methyl hydrogen, and the peak at 5.1 ppm corresponds to methylene hydrogen of the PLLA segment (**Figure 1**). The peak of 1750 cm^{-1} corresponds to the stretch vibration absorption of carbonyl of the PLLA segment. The peaks at 2,996 and 2,946 cm^{-1} are assigned to the stretching vibration peak of the methyl and the methylene, respectively. The peaks near 1,180 and 1,140 cm^{-1} are assigned to the stretching vibration peak of C-O-C. The peak near 1,448 cm^{-1} is assigned to the bending vibration absorption peak of CH (**Figure 2**).

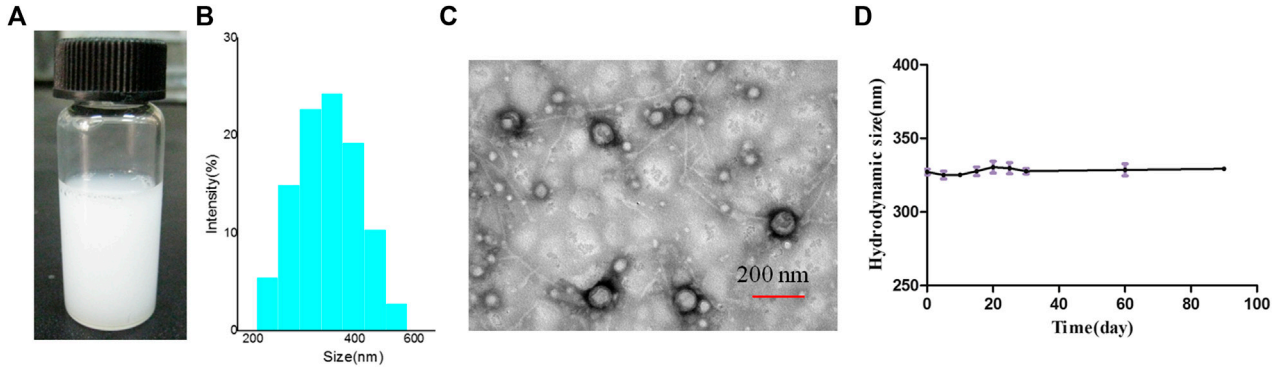

Figure 3 | Characterization of Lf–PLLA NBs. **(A)** Appearance, **(B)** size distribution, **(C)** TEM images, and **(D)** the stability of the NBs *in vitro*.

PLLA nanobubbles were prepared by a double-emulsion (O_1/O_2/W) process as described in our previous works (Luo et al., 2015). Liquid PFP, the boiling point of which at atmospheric pressure is 28.5°C, was encapsulated by the material of the PLLA and developed the structure of core shell. The hydrophobic nature of PLLA could have delayed solution penetration, which retards the outward diffusion of PFP in the core of nanobubbles; furthermore, the liquid PFP enhanced the storage stability compared to other gases. Under the irradiation of the ultrasound wave, the liquid PFP in the core of nanobubbles undergoes phase transition and becomes gaseous PFP at physiological temperature, which ensured the effect of enhanced ultrasound imaging. NB suspension was mixed with α-maleimidyl-ω-N-hydroxysuccinimidylpoly (ethylene glycol) (NHS-PEG-MAL) solution; the mixture was further incubated with Lf-SH in PBS at room temperature. Thus, lactoferrin of tumor-targeting ligand was conveniently conjugated onto the surface of the nanobubbles. The method used here was described in our previously published work (Luo et al., 2015).

The average hydrodynamic diameter and zeta potential of Lf–PLLA nanobubbles were measured by dynamic light scattering, and the results are shown in **Figure3**. The average size of nanobubbles was 315.3 ± 4.2 nm, and the polydispersity index (PDI) was 0.153 ± 0.020, indicating the size of nanobubbles was relatively uniform. The zeta potential was assessed, and the results showed that the Lf–PLLA nanobubbles had a negative charge of −11.3 ± 0.2 mV. TEM was used to observe the morphology and size of nanobubbles. Obviously, Lf–PLLA NBs appeared to have spherical shape and were quite dispersed with a diameter of about 140.3 ± 3.5 nm, smaller than the hydrated particle size measured by dynamic light scattering. In addition, the core shell structure of nanobubbles was apparently confirmed from the TEM images. Lf–PLLA nanobubbles were stored at 4°C for 90 days to test their stability determined by detecting the changes in particle size and potential, and the results are shown in **Figure 3D**. No significant change was observed during 90 days of storage (0, 5, 10, 15, 20, 25, 30, and 90 days), indicating the Lf–PLLA nanobubbles had a good physical stability at low temperatures.

The cytotoxicity of the Lf–PLLA nanobubbles was evaluated by HL7702 cells incubated with nanobubbles at all evaluated concentrations for 24 h. The results are shown in **Figure 4A**. At the evaluated concentration range (0.5–20.0%, v/v), there were no apparent effects on the cell viability of HL7702, which showed that Lf–PLLA nanobubbles had little cytotoxicity to the HL7702 cells. The results of the hemolysis assay are shown in **Figure 4B**, and the hemolysis rate value of all testing samples was less than 5%, which indicated that Lf–PLLA nanobubbles had no obvious effect on the hemolysis rate. The above results indicated that the Lf–PLLA nanobubbles had good biocompatibility and were a potential carrier for biomedical applications.

The boiling point of PFP is 28.5°C at atmospheric pressure. However, its boiling point changes when it is encapsulated in the capsule and stabilized by elastic polymer shells. The PFP in the nanobubbles did not undergo a phase transition at 37°C due to the Laplace pressure, and its boiling temperature would be substantially elevated. The Laplace pressure is the differential pressure of bubbles between its interior and exterior, which is caused by surface tension. Laplace pressure is given as follows:

$$\Delta P = P_{\text{inside}} - P_{\text{outside}} = 2\sigma/r$$

where r is the radius of the bubble and σ is the solid–liquid interfacial tension (German et al., 2016). The change in pressure between the internal and external of bubbles is proportional to the surface tension and inversely proportional to the bubble radius. The smaller the particle size of nanobubbles prepared by the same carrier material is, the greater the Laplace pressure will be, which may lead to an elevation of the boiling point of the internal liquid. The hydrophobicity of liquid PFPs has high interfacial tension in water; in addition, the size of nanobubbles is small, which would result in the increase in the Laplace pressure of the liquid core.

Ultrasound-induced phase transition is called acoustic droplet vaporization (ADV). The experiments of the ADV threshold were carried out. The NBs in the latex gloves were immersed in a thermostatic water bath. The initial temperature of the water was set to 23°C, the 10 MHz probe was close to the latex gloves, and ultrasonic images were collected. Then , the temperature was set to 25°C and maintained for 2 min. In the meantime, the probe was

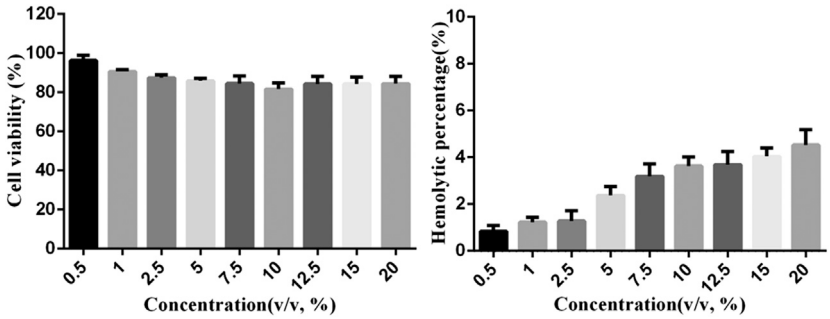

Figure 4 | (A) *In vitro* cytotoxicity with the MTT assay. *In vitro* cell viability of HL7702 cell incubated with nanobubbles at different concentrations for 24 h. Data were reported as mean ± SD (n = 5). **(B)** *In vitro* hemolysis experiment. The hemolysis rate of erythrocyte suspensions incubated with nanobubbles. Data were reported as mean ± SD (n = 5).

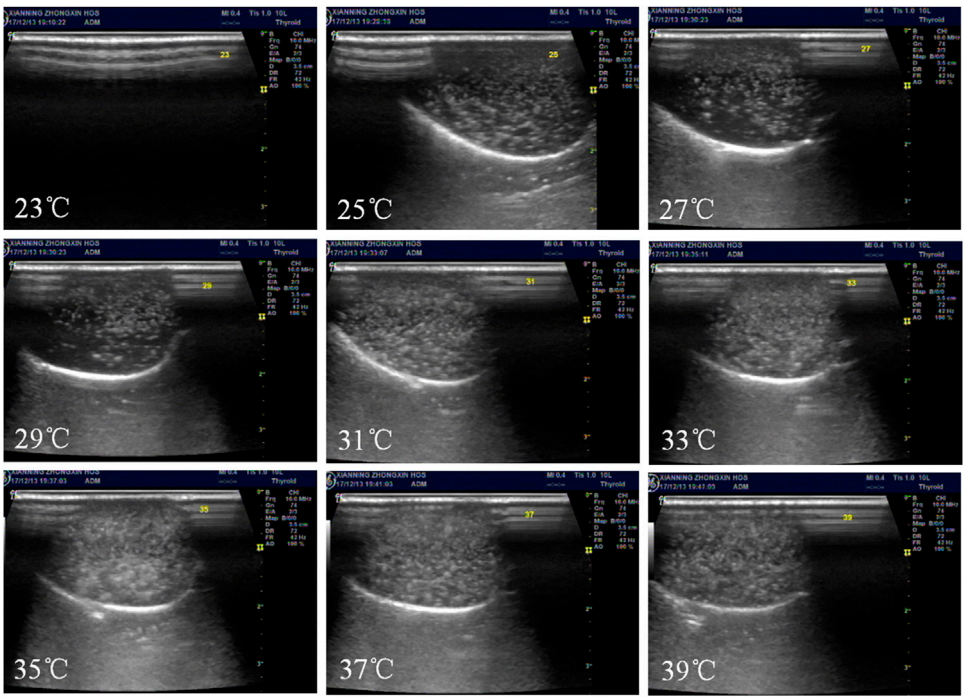

Figure 5 | *In vitro* ultrasonic images of Lf–PLLA NBs in latex gloves mold. Temperature was increased from 23 to 39°C at an interval of 2°C.

closed to gloves and collected ultrasonic imaging with B-mode images. Similarly, the temperature rose to 39°C gradually.

The results are shown in **Figures 5**, **6**. The collected image had few bright spots at 23°C; however, the bright spots augmented a lot at 25°C. As the temperature increased, the number of bright spots gradually increased. When the temperature rose to 35°C, the bright spots reached a maximum and then began to decrease. Theoretically, the two most important factors for the droplet to bubble transitions are temperature and ultrasound wave. In this study, the droplet-to-bubble transitions started at 25°C under ultrasound radiation.

The PFP in the nanobubbles undergo the droplet-to-bubble transitions, and the nanobubbles become bigger nano- or microbubbles. Gases of PFP stabilized by elastic polymer shells are compressible. Under ultrasonic radiation, nanoscale bubbles expand and contract rhythmically, which will produce a harmonic signal. However, the tissue is almost incompressible, and there is no harmonic signal. Some pulse sequences are used to separate the differences of these signals and display them on a screen.

The shell material of the nanobubbles was the PLLA polymer, which has good mechanical properties and stretches under the ultrasound radiation. As shown in **Figure 7**, the Lf–PLLA nanobubbles in the latex gloves oscillated and produced the harmonic signal, and many bright spots reflected the harmonic signal appeared in the image of the ultrasound.

However, when saline and ultrasound medicinal coupling gel were placed in the latex gloves, no signal was observed. Through the experiment, it could be proved that NBs had acoustic properties.

Ultrasound-facilitated drug/gene delivery using bubbles has attracted widespread attention (Yin et al., 2014; Zhang et al., 2014; Xie et al., 2016b; Cai et al., 2018). This technology is safe, effective, and noninvasive. The contrast agent, such as nano- and microbubbles, is usually a vector system. Under ultrasound irradiation, nano- and microbubbles will be expanded and contracted. Once the ultrasound intensity reaches a certain level, the bubbles will be immediately destroyed. This will produce the mechanical effect and transient cavitation effect to perturb cell membranes and cause transient pores in the target area, which facilitates drug/gene entry into the cell. The destruction threshold of bubbles is associated with the property of materials. Lipid-based shell material slacking active sites for conjugating tumor-targeting molecules generally possess a low destruction threshold, while polymer-based shell materials, especially the stiff polymeric shell, having a high destruction threshold under ultrasonic irradiation, will not oscillate actively. The shell material of the nanobubbles was the PLLA polymer, whose molecular weight was appropriate and could be effectively destroyed by ultrasonication. As shown in **Figure 8**, compared with no crush treatment (**Figure 8A**), the signal intensity of crush treatment (**Figure 8B**) dropped significantly. Furthermore, many new larger bright spots appeared at the bottom (**Figure 8B**). Some nanobubbles collapsed in the ultrasound field, which would lead to a reduction in the number of nanobubbles. At the same time, ultrasound also induced nanobubbles coalescence into larger microbubbles. As a result, Lf–PLLA nanobubbles might be served as a novel nonviral drug/gene delivery system.

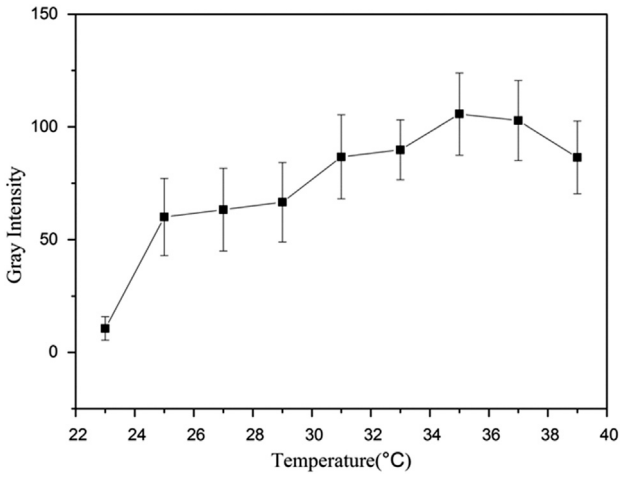

Figure 6 | Representative *in vitro* ultrasonic images. Quantitative gray-scale for the ultrasonic intensity of Lf–PLLA nanobubbles from 23 to 39°C.

To evaluate the enhanced ultrasonic imaging effect of nanobubbles on the tumor *in vivo*, six animal models of nude mice bearing subcutaneous tumors were studied. Before drug administration , tumor ultrasonic images of nude mice were collected for control. The tumor was a dark hypoechoic area and had obscure boundaries with surrounding tissues (**Figure 9A**). Subsequently, the Lf–PLLA nanobubbles (100 μl) solution was injected, the tumor turned bright, and the boundaries became obvious (**Figure 9B**), and the enhanced ultrasound imaging lasted about 1 h, which was longer than that reported in the literature (Oda et al., 2015; Du et al., 2018). The results showed that the Lf–PLLA nanobubbles could enhance ultrasound imaging of tumors.

CONCLUSIONS

In this study, a novel biocompatible ultrasound contrast agent was developed, using poly(L-lactide) polymer synthesized by ring-opening polymerization reaction as shell material, with a traditional double-emulsion solvent evaporation method. Targeted modification of PLLA nanobubbles with Lf was

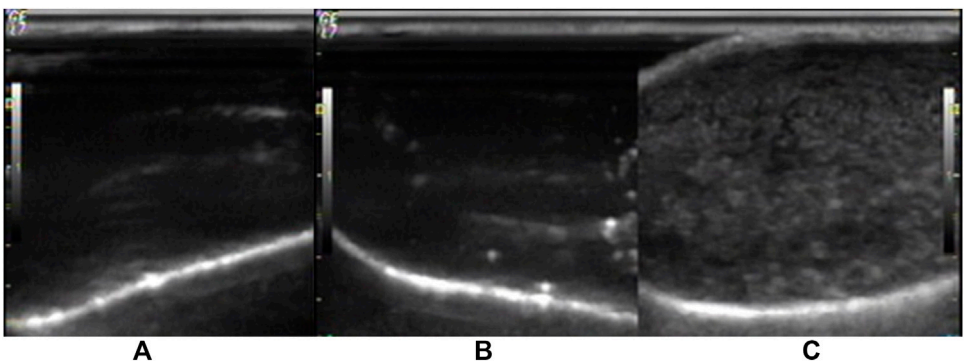

Figure 7 | Representative *in vitro* ultrasonic images. **(A)** Saline, **(B)** ultrasonic medicinal coupling gel, **(C)** nanobubbles under high-frequency diagnostic ultrasound in latex gloves mold.

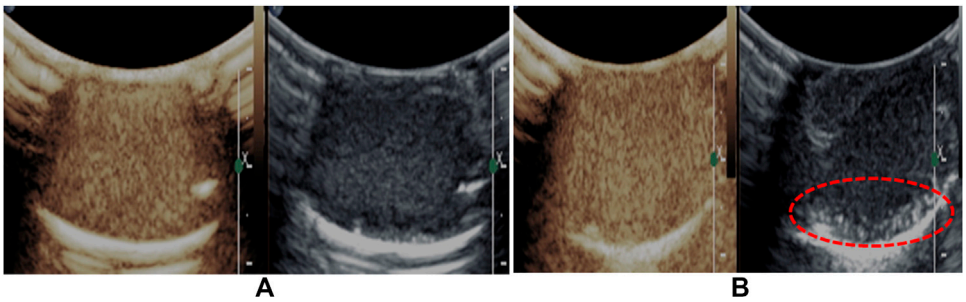

Figure 8 | Representative *in vitro* ultrasonic images. **(A)** Precrush and **(B)** postcrush of the nanobubbles upon high-frequency ultrasound exposure.

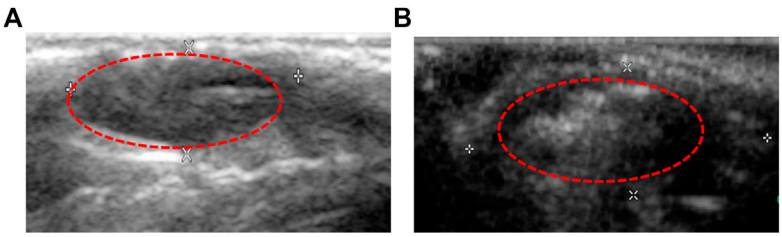

Figure 9 | Ultrasound images of the subcutaneous tumor in BALB/c nude mice. **(A)** and **(B)** are before and after injection of Lf–PLLA NBs.

carried out. The biocompatible results indicated that the Lf–PLLA nanobubbles had little cytotoxicity and hemolysis. The Lf–PLLA nanobubbles had shown they could enhance the ability of ultrasound imaging *in vitro* and *in vivo*. Our results suggest that Lf–PLLA nanobubbles represent a promising nano-sized ultrasound contrast agent.

DATA AVAILABILITY STATEMENT

The raw data supporting the conclusions of this article will be made available by the authors, without undue reservation.

ETHICS STATEMENT

The animal study was reviewed and approved by the Animal Experimentation Ethics Committee of the Hubei University of Science and Technology and carried out in accordance with guidelines approved by the Science and Technology Department of Hubei Province.

AUTHOR CONTRIBUTIONS

BL and JC designed the work and wrote the manuscript. RX, LH, and HW carried out the experiments. ZZ and LPH performed the experiments of ultrasonic imaging.

FUNDING

This work was financially supported by the Funds of Science and Technology Department of Hubei Province (2018CFB533), Health and Family Planning Commission Project of Hubei Province (WJ2017Q042, WJ2017M252), and Initial Scientific Research Fund of Ph.D. in the Hubei University of Science and Technology (BK1511).

REFERENCES

Cai, J., Qian, K., Zuo, X., Yue, W., Bian, Y., Yang, J., et al. (2019). PLGA nanoparticle-based docetaxel/LY294002 drug delivery system enhances antitumor activities against gastric cancer. *J. Biomater. Appl.* 33(10), 1394–1406. doi:10.1177/0885328219837683

Cai, W. B., Yang, H. L., Zhang, J., Yin, J. K., Yang, Y. L., Yuan, L. J., et al. (2015). The optimized fabrication of nanobubbles as ultrasound contrast agents for tumor imaging. *Sci. Rep.* 5, 13725. doi:10.1038/srep13725

Cai, W., Lv, W., Feng, Y., Yang, H., Zhang, Y., Yang, G., et al. (2018). The therapeutic effect in gliomas of nanobubbles carrying siRNA combined with ultrasound-targeted destruction. *Int. J. Nanomed.* 13, 6791–6807. doi:10.2147/IJN.S164760

Dinh Nguyen, T., Feng, G., Yi, X., Lyu, Y., Lan, Z., Xia, J., et al. (2018). Six-month evaluation of novel bioabsorbable scaffolds composed of poly-L-lactic acid and amorphous calcium phosphate nanoparticles in porcine coronary arteries. *J. Biomater. Appl.* 33(2), 227–233. doi:10.1177/0885328218790332

Du, J., Li, X. Y., Hu, H., Xu, L., Yang, S. P., and Li, F. H. (2018). Preparation and imaging investigation of dual-targeted C3F8-filled PLGA nanobubbles as a

novel ultrasound contrast agent for breast cancer. *Sci. Rep.* 8(1), 3887. doi:10.1038/s41598-018-21502-x

Duan, S., Guo, L., Shi, D., Shang, M., Meng, D., and Li, J. (2017). Development of a novel folate-modified nanobubbles with improved targeting ability to tumor cells. *Ultrason. Sonochem.* 37, 235–243. doi:10.1016/j.ultsonch.2017.01.013

Gao, Y., Hernandez, C., Yuan, H. X., Lilly, J., Kota, P., Zhou, H., et al. (2017). Ultrasound molecular imaging of ovarian cancer with CA-125 targeted nanobubble contrast agents. *Nanomed. Nanotechnol. Biol. Med.* 13(7), 2159–2168. doi:10.1016/j.nano.2017.06.001

German, S. R., Edwards, M. A., Chen, Q., and White, H. S. (2016). Laplace pressure of individual H2 nanobubbles from pressure–addition electrochemistry. *Nano Lett.* 16(10), 6691–6694. doi:10.1021/acs.nanolett.6b03590

Guvener, N., Appold, L., de Lorenzi, F., Golombek, S. K., Rizzo, L. Y., Lammers, T., et al. (2017). Recent advances in ultrasound-based diagnosis and therapy with micro- and nanometer-sized formulations. *Methods* 130, 4–13. doi:10.1016/j.ymeth.2017.05.018

He, P., Yan, H., Zhao, J., Gou, M., and Li, X. (2019). An evaluation of the wound healing potential of tetrahydrocurcumin-loaded MPEG-PLA nanoparticles. *J. Biomater. Appl.* 885328219851195. doi:10.1177/0885328219851195

Ji, G., Yang, J., and Chen, J. (2014). Preparation of novel curcumin-loaded multifunctional nanodroplets for combining ultrasonic development and targeted chemotherapy. *Int. J. Pharm.* 466(1-2), 314–320. doi:10.1016/j.ijpharm.2014.03.030

Li, J., Tian, Y., Shan, D., Gong, A., Zeng, L., Ren, W., et al. (2017a). Neuropeptide Y Y1 receptor-mediated biodegradable photoluminescent nanobubbles as ultrasound contrast agents for targeted breast cancer imaging. *Biomaterials* 116, 106–117. doi:10.1016/j.biomaterials.2016.11.028

Li, Y., Wan, J., Zhang, Z., Guo, J., and Wang, C. (2017b). Targeted soft biodegradable Glycine/PEG/RGD-Modified poly(methacrylic acid) nanobubbles as intelligent theranostic vehicles for drug delivery. *ACS Appl. Mater. Interfaces* 9(41), 35604–35612. doi:10.1021/acsami.7b11392

Luo, B., Liang, H., Zhang, S., Qin, X., Liu, X., Liu, W., et al. (2015). Novel lactoferrin-conjugated amphiphilic poly(aminoethyl ethylene phosphate)/poly(L-lactide) copolymer nanobubbles for tumor-targeting ultrasonic imaging. *Int. J. Nanomed.* 10, 5805–5817. doi:10.2147/IJN.S83582

Meng, M., Gao, J., Wu, C., Zhou, X., Zang, X., Lin, X., et al. (2016). Doxorubicin nanobubble for combining ultrasonography and targeted chemotherapy of rabbit with VX2 liver tumor. *Tumour Biol.* 37(7), 8673–8680. doi:10.1007/s13277-015-4525-5

Nishimura, K., Fumoto, S., Fuchigami, Y., Hagimori, M., Maruyama, K., and Kawakami, S. (2017). Effective intraperitoneal gene transfection system using nanobubbles and ultrasound irradiation. *Drug Delivery* 24(1), 737–744. doi:10.1080/10717544.2017.1319433

Oda, Y., Suzuki, R., Mori, T., Takahashi, H., Natsugari, H., Omata, D., et al. (2015). Development of fluorous lipid-based nanobubbles for efficiently containing perfluoropropane. *Int. J. Pharm.* 487(1-2), 64–71. doi:10.1016/j.ijpharm.2015.03.073

Perera, R. H., Solorio, L., Wu, H., Gangolli, M., Silverman, E., Hernandez, C., et al. (2013). Nanobubble ultrasound contrast agents for enhanced delivery of thermal sensitizer to tumors undergoing radiofrequency ablation. *Pharmaceut. Res.* 31(6), 1407–1417. doi:10.1007/s11095-013-1100-x

Song, Z., Wang, Z., Shen, J., Xu, S., and Hu, Z. (2017). Nerve growth factor delivery by ultrasound-mediated nanobubble destruction as a treatment for acute spinal cord injury in rats. *Int. J. Nanomed.* 12, 1717–1729. doi:10.2147/IJN.S128848

Tonietto, L., Vasquez, A. F., Dos Santos, L. A., and Weber, J. B. (2019). Histological and structural evaluation of growth hormone and PLGA incorporation in macroporous scaffold of alpha-tricalcium phosphate cement. *J. Biomater. Appl.* 33(6), 866–875. doi:10.1177/0885328218812173

Tranquart, F., Bettinger, T., and Hyvelin, J. M. (2014). Ultrasound and microbubbles for treatment purposes: mechanisms and results. *Clin. Transl. Imaging* 2(1), 89–97. doi:10.1007/s40336-014-0052-4

Wang, J. F., Wu, C. J., Zhang, C. M., Qiu, Q. Y., and Zheng, M. (2009). Ultrasound-mediated microbubble destruction facilitates gene transfection in rat C6 glioma cells. *Mol. Biol. Rep.* 36(6), 1263–1267. doi:10.1007/s11033-008-9307-3

Wu, M., Wang, Y., Wang, Y., Zhang, M., Luo, Y., Tang, J., et al. (2017). Paclitaxel-loaded and A10-3.2 aptamer-targeted poly(lactide-co-glycolic acid) nanobubbles for ultrasound imaging and therapy of prostate cancer. *Int. J. Nanomed.* 12, 5313–5330. doi:10.2147/IJN.S136032

Wu, M., Zhao, H., Guo, L., Wang, Y., Song, J., Zhao, X., et al. (2018). Ultrasound-mediated nanobubble destruction (UMND) facilitates the delivery of A10-3.2 aptamer targeted and siRNA-loaded cationic nanobubbles for therapy of prostate cancer. *Drug Delivery* 25(1), 226–240. doi:10.1080/10717544.2017.1422300

Xie, X., Lin, W., Li, M., Yang, Y., Deng, J., Liu, H., et al. (2016a). Efficient siRNA delivery using novel cell-penetrating peptide-siRNA conjugate-loaded nanobubbles and ultrasound. *Ultrasound Med. Biol.* 42(6), 1362–1374. doi:10.1016/j.ultrasmedbio.2016.01.017

Xie, X., Lin, W., Liu, H., Deng, J., Chen, Y., Liu, H., et al. (2016b). Ultrasound-responsive nanobubbles contained with peptide-camptothecin conjugates for targeted drug delivery. *Drug Delivery* 23(8), 2756–2764. doi:10.3109/10717544.2015.1077289

Yang, H., Cai, W., Xu, L., Lv, X., Qiao, Y., Li, P., et al. (2015a). Nanobubble-Affibody: novel ultrasound contrast agents for targeted molecular ultrasound imaging of tumor. *Biomaterials* 37, 279–288. doi:10.1016/j.biomaterials.2014.10.013

Yang, H., Deng, L., Li, T., Shen, X., Yan, J., Zuo, L., et al. (2015b). Multifunctional PLGA nanobubbles as theranostic agents: combining doxorubicin and P-gp siRNA Co-delivery into human breast cancer cells and ultrasound cellular imaging. *J. Biomed. Nanotechnol.* 11(12), 2124–2136. doi:10.1166/jbn.2015.2168

Yao, Y., Yang, K., Cao, Y., Zhou, X., Xu, J., Liu, J., et al. (2016). Comparison of the synergistic effect of lipid nanobubbles and SonoVue microbubbles for high intensity focused ultrasound thermal ablation of tumors. *PeerJ* 4, e1716. doi:10.7717/peerj.1716

Yin, T., Wang, P., Li, J., Wang, Y., Zheng, B., Zheng, R., et al. (2014). Tumor-penetrating codelivery of siRNA and paclitaxel with ultrasound-responsive nanobubbles hetero-assembled from polymeric micelles and liposomes. *Biomaterials* 35(22), 5932–5943. doi:10.1016/j.biomaterials.2014.03.072

Zhang, L., Liu, Y., Xiang, G., Lv, Q., Huang, G., Yang, Y., et al. (2011). Ultrasound-triggered microbubble destruction in combination with cationic lipid microbubbles enhances gene delivery. *J. Huazhong Univ. Sci. Technol.* 31(1), 39–45. doi:10.1007/s11596-011-0147-3

Zhang, X., Zheng, Y., Wang, Z., Huang, S., Chen, Y., Jiang, W., et al. (2014). Methotrexate-loaded PLGA nanobubbles for ultrasound imaging and Synergistic Targeted therapy of residual tumor during HIFU ablation. *Biomaterials* 35(19), 5148–5161. doi:10.1016/j.biomaterials.2014.02.036

Zhao, Y.-Z., and Lu, C.-T. (2007). Factors that affect the efficiency of antisense oligodeoxyribonucleotide transfection by insonated gas-filled lipid microbubbles. *J. Nanoparticle Res.* 10(3), 449–454. doi:10.1007/s11051-007-9274-y

Zhou, T., Cai, W., Yang, H., Zhang, H., Hao, M., Yuan, L., et al. (2018). Annexin V conjugated nanobubbles: a novel ultrasound contrast agent for *in vivo* assessment of the apoptotic response in cancer therapy. *J. Contr. Release.* 276, 113–124. doi:10.1016/j.jconrel.2018.03.008

Zhu, L., Guo, Y., Wang, L., Fan, X., Xiong, X., Fang, K., et al. (2017). Construction of ultrasonic nanobubbles carrying CAIX polypeptides to target carcinoma cells derived from various organs. *J. Nanobiotechnol.* 15(1), 63. doi:10.1186/s12951-017-0307-0

Zhu, L., Wang, L., Liu, Y., Xu, D., Fang, K., and Guo, Y. (2018). CAIX aptamer-functionalized targeted nanobubbles for ultrasound molecular imaging of various tumors. *Int. J. Nanomed.* 13, 6481–6495. doi:10.2147/IJN.S176287

Conflict of Interest: The authors declare that the research was conducted in the absence of any commercial or financial relationships that could be construed as a potential conflict of interest.